

Particokinetics: computational analysis of the superparamagnetic iron oxide nanoparticles deposition process

Walter HZ Cárdenas
Javier B Mamani
Tatiana T Sibov
Cristofer A Caous
Edson Amaro Jr
Lionel F Gamarra

Instituto do Cérebro, Hospital
Israelita Albert Einstein, São Paulo,
Brazil

Background: Nanoparticles in suspension are often utilized for intracellular labeling and evaluation of toxicity in experiments conducted *in vitro*. The purpose of this study was to undertake a computational modeling analysis of the deposition kinetics of a magnetite nanoparticle agglomerate in cell culture medium.

Methods: Finite difference methods and the Crank-Nicolson algorithm were used to solve the equation of mass transport in order to analyze concentration profiles and dose deposition. Theoretical data were confirmed by experimental magnetic resonance imaging.

Results: Different behavior in the dose fraction deposited was found for magnetic nanoparticles up to 50 nm in diameter when compared with magnetic nanoparticles of a larger diameter. Small changes in the dispersion factor cause variations of up to 22% in the dose deposited. The experimental data confirmed the theoretical results.

Conclusion: These findings are important in planning for nanomaterial absorption, because they provide valuable information for efficient intracellular labeling and control toxicity. This model enabled determination of the *in vitro* transport behavior of specific magnetic nanoparticles, which is also relevant to other models that use cellular components and particle absorption processes.

Keywords: Magnetite, nanoparticles, diffusion, sedimentation, agglomerates, computational modeling, cellular labeling, magnetic resonance imaging

Introduction

Efficient internalization of nanoparticles of diverse sizes and shapes continues to be studied widely at a molecular level with respect to the interaction of nanoparticles with cellular elements. Increasing biomedical applications are being found for superparamagnetic iron oxide nanoparticles (SPIONs). These magnetic particles have great potential for labeling intracellular elements showing early life events triggered by biochemical pathways. They may also assist in obtaining a correct diagnostic result and determining appropriate treatment.¹⁻³ Because of their physicochemical properties, labeled SPIONs are suitable for use in cell monitoring during imaging procedures *in vivo*.⁴⁻¹⁰ In addition, SPIONs can be used in immunolocalization assays to identify cancer cells and micrometastases, and as a consequence, enable an earlier definitive diagnosis.¹¹ Furthermore, their cellular internalization processes in tumor tissue may facilitate tumor eradication in the near future, if focal cellular lysis can be achieved using magnetic hyperthermia.¹²⁻¹⁵ In general, SPIONs used for cell tagging have a biocompatible covering and the internalization process occurs via endocytosis.¹⁶ Theoretical and experimental investigations of endocytosis suggest preferential

Correspondence: Walter Humberto
Zavala Cárdenas
Instituto do Cérebro, Hospital Israelita
Albert Einstein, Av Albert Einstein,
627/701, Piso Chinuch (2S),
Morumbi, São Paulo/SP,
Brazil, CEP 05651-901
Tel +55 11 21512044
Fax +55 11 3813 4334
Email walter.cardenas@einstein.br

absorption of magnetic nanoparticles ranging in size between 20 nm and 100 nm. Despite all the knowledge acquired so far, our scientific understanding of how cells interact with nanoparticles of different sizes is incomplete.

Research on cells in culture in vitro, along with toxicity studies, have been undertaken for novel compounds.^{17,18} The cell culture consists of a set of adherent proliferating cells constrained to a recipient in an appropriate cell culture medium. For intracellular labeling, the culture medium should contain a quantity of SPIONs that, in accordance with diffusion and sedimentation processes, is able to reach the bottom of the recipient in order to permit evaluation of the effect of a nanoparticle dose.² However, in vitro assays for SPIONs labeling present some challenges because of the presence of solid compounds. These particles do not behave in the same manner as soluble molecules. The latter are able to diffuse, sediment, and agglomerate depending on their size, shape, and density, so the concentration of SPIONs on the cell surface may be more important than the concentration in the culture medium, leading to increased absorption of SPIONs by cells. As a consequence, the sedimentation, agglomeration, diffusion, and stability of SPIONs depend on their physicochemical characteristics, as well as the composition and characteristics of the cell culture medium. Some physicochemical properties of SPIONs, such as ionic force, have an influence on their dispersive stability, altering the double electric layer thickness, while changes in pH affects their dispersion state and surface charge, ie, zeta potential.

Ion adsorption and polymeric capping on the nanoparticle surface may contribute to agglomeration and dispersion stability, with repulsive electrostatic interaction prevailing over Van der Waals forces, causing slower agglomeration.¹⁹ The stability of SPIONs depends primarily on steric force which is related directly to the polymeric layer on the surface of the nanoparticle. The complexity of this type of dispersion leads to difficulty in defining a mathematical expression that accurately reflects dose absorption by cells. The definition of dose absorbed per nanoparticle in an in vitro system is dynamic and complex, and is not comparable with that of any other type of particle.²⁰ Experimental and theoretical studies have shown that the size of nanoparticles targeted to cells is an essential parameter for determining the number of nanoparticles which gain entry into the cells.^{21–23} All these processes need to be understood fully to be able to analyze the effects of the characteristics of the nanoparticles and the medium, as well as to use SPIONs correctly for appropriate intracellular tagging.

Qualitative understanding of this dynamic deposition process is challenging. A theoretical model may help to elucidate the deposition of subjacent mechanisms. Mathematical expressions related to the convection-diffusion transport equation for nanoparticles deposited in a suspension or liquid medium, involve parabolic-type partial derivatives. These expressions describe the variability in nanoparticle concentration in terms of the effects of diffusion and convection. Three distinct methods may be used to study cell populations in culture, considering the concentration of the nanoparticles located adjacent to the cells, ie, experimental design, analytical and computational methods. We used the computational method for this research. Mathematical simplifications must be performed to achieve accurate computational modeling to solve partial differential equations. The main purpose of using numerical methods is for discretization of the continuum that becomes finite, making the computational solution viable. The aim is to optimize the set of equations regarding techniques intended to clarify and predict novel properties, thereby reducing considerably the financial costs of research. The purpose of this research was to simulate in vitro transport and motion as well as the deposition rate of SPIONs on the cell surface, addressing several parameters including temperature, height, particle size in solution, state of agglomeration, and density.

Understanding and control of the process by which SPIONs gain entry into cells is critical for a diverse set of applications. The present work aimed to determine the ideal conditions for cell labeling based on in vitro deposition of SPIONs. The Crank–Nicolson algorithm was used to solve the convective-diffusion equation by the finite difference method for obtaining the solution to a parabolic-type partial differential equation.

Materials and methods

Formulation of the problem

In vitro deposition of magnetic nanoparticles is a common technique used in cellular internalization processes and depends on diffusion of suspended particles and convection processes regarding size and specific mass according to Stokes' law and the Stokes–Einstein equation.

The density and viscosity of the medium interfere with diffusion, sedimentation, and agglomeration processes according to the size, shape, density, and/or electric charge of the particle. In order to test if these characteristics significantly affect the dose absorbed by the cell, it is important to estimate the effective dose delivered to the cell

surface. Figure 1 shows a schema explaining how SPIONs suspended in a liquid medium are transported to the bottom of the recipient as a result of a series of competitive effects involving dispersion of the nanoparticles in the volume of the recipient (ie, diffusion) and macroscopic concentration of nanoparticles related to the presence of velocity fields oriented along a concentration gradient (convection). The latest effect of mass transport is designated as natural convection if the resulting dispersion was caused by external factors, such as gravitational force (ie, gravitational sedimentation).

The deposition process for magnetic nanoparticles was modeled on the basis of the following assumptions: nanoparticles are monodispersed and of spherical shape; the thermophysical properties are constant during the entire period of exposure; the colloidal suspension of nanoparticles is in a homogenous and isotropic medium; a constant diffusion coefficient; mass transportation occurring at a mean settling velocity; the contour condition at the bottom ($z = L$) of the recipient is of a convective type; and a moving laminar flow system with a low Reynolds index (<100) decreasing the effect of its own weight, as well as that of the nanoparticles surrounding the collision points. The concentration of a given nanoparticle suspension that has reached its terminal velocity was obtained by average concentrations measured at determined time intervals $C[h(t)]$, where $h(t)$ is the precipitated concentration distance of nanoparticles in a period of time t , as schematized in Figure 2.

The experiment consists of the distance h measured between the upper edge of the tube and the meniscus as a function of time, t . The plot of h is a function of time, t root square is a straight line; from the slope of the straight line we obtain the diffusion coefficient. Graphs of $C[h(t)]$ as a function of z or t may also be developed. The theoretical relationship between the particle diameter and the time that

the particle takes to move a determined distance (diffusion effect) is given by the Einstein–Smoluchowski equation:

$$t = \frac{\langle x^2 \rangle}{2D} \quad (1)$$

where t is mean time (some particles take a shorter or longer length of time to reach the cells), $\langle x^2 \rangle$ is the root square of the mean quadratic distance or mean distance that the particle should move, and D is the diffusion coefficient, depending on the diameter obtained by the Stokes–Einstein equation:

$$D = \frac{RT}{3N_A \pi \mu d_p} \quad (2)$$

where R represents the ideal gas constant and T is the temperature of the medium, N_A is Avogadro's number, μ is the viscosity, and d_p is the hydrodynamic particle diameter. A low Reynolds number implies a laminar flow system, reflecting relative velocity among the nanoparticles and the medium inferior to the critical value. In this scenario, the resistance produced by the medium is caused almost exclusively by frictional forces that oppose the sliding of the layers of fluid on the other from the boundary layer adhered to the particle surface. If the particles are following vertically in a viscous fluid, because of its weight, the settling velocity may be calculated, with the frictional force and the gravity force being made equal. The settling velocity is obtained from Stokes' Law as:

$$V = \frac{g(\rho_p - \rho_f)d_p^2}{18\mu} \quad (3)$$

Where g is the standard gravity, and ρ_p and ρ_f are the relative densities of the particle and fluid, respectively. The period of time used to travel the same distance due to gravitational

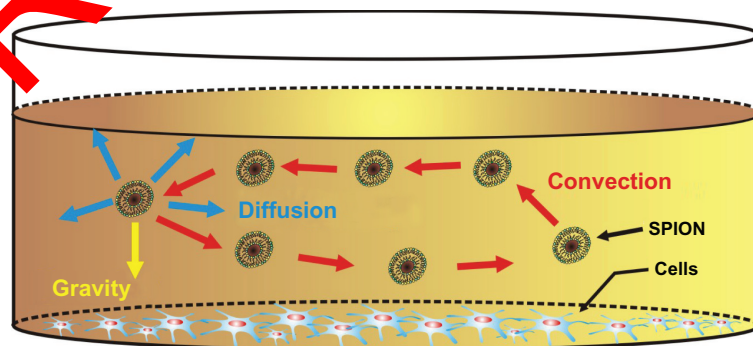


Figure 1 Representation of process of SPION deposition and cellular internalization.

Notes: The result of diffusion and gravitational sedimentation effects guide particle deposition at the bottom of the recipient. Positioning at the boundary of the cellular surfaces is essential for internalization and labeling of the absorbed dose.

Abbreviation: SPION, superparamagnetic iron oxide nanoparticle.

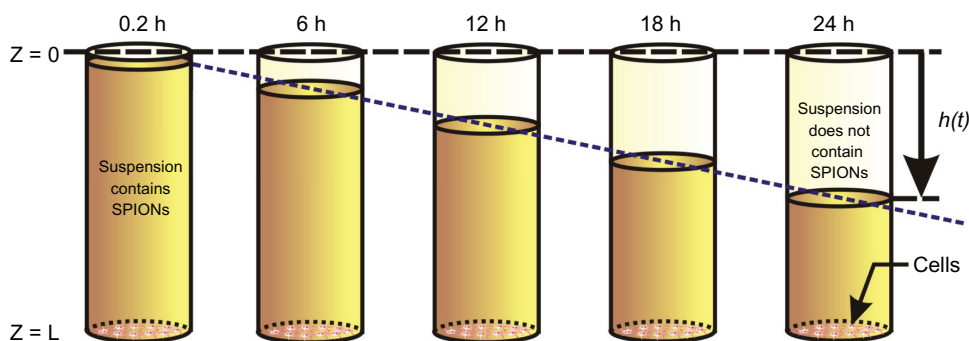


Figure 2 Discrete deposition of SPIONs in suspension that reach their terminal settling velocity, v_{term} .

Notes: In the figure, z represents the generic coordinate for depth, where $z = 0$, and $z = L$ characterizes the top and the bottom of the recipient, respectively. $h(t)$ is the distance particles have fallen down by in a period of time t , computed as $v_{term} \cdot t$.

Abbreviation: SPIONs, superparamagnetic iron oxide nanoparticles.

sedimentation is given by the relationship $t = x/V$. Note that D is an inverse function of particle size and not a function of the density between the particle and the medium, and V is a function proportional to the square of the particle diameter.

Figure 3 shows the typical time it would take a SPION of Fe_3O_4 to propagate by diffusion (red line) or sedimentation (blue line) for a distance of 1 mm through an aqueous solution, with characteristics of the cell culture medium as a function of the diameter of the nanoparticle. The distance is similar to the depth of the culture medium used in intracellular labeling trials. The intersection of diffusion and sedimentation transport occurs at 75 nm. Diffusion

transport is facilitated by nanoparticles smaller than 75 nm in diameter, while the sedimentation method is appropriate for nanoparticles of larger diameter. Moreover, particle diffusion reflects transport of nanoparticles in suspension in the presence of a concentration gradient. When the diffusion coefficient becomes inversely proportional to the size of the particle, deposition by diffusion becomes less relevant for large particles ($d > 100$ nm).

In contrast, a suspension of particles can spread, deposit, or agglomerate according to their size and density. These processes are expected to affect the dose deposited significantly. The definition of dose for particles

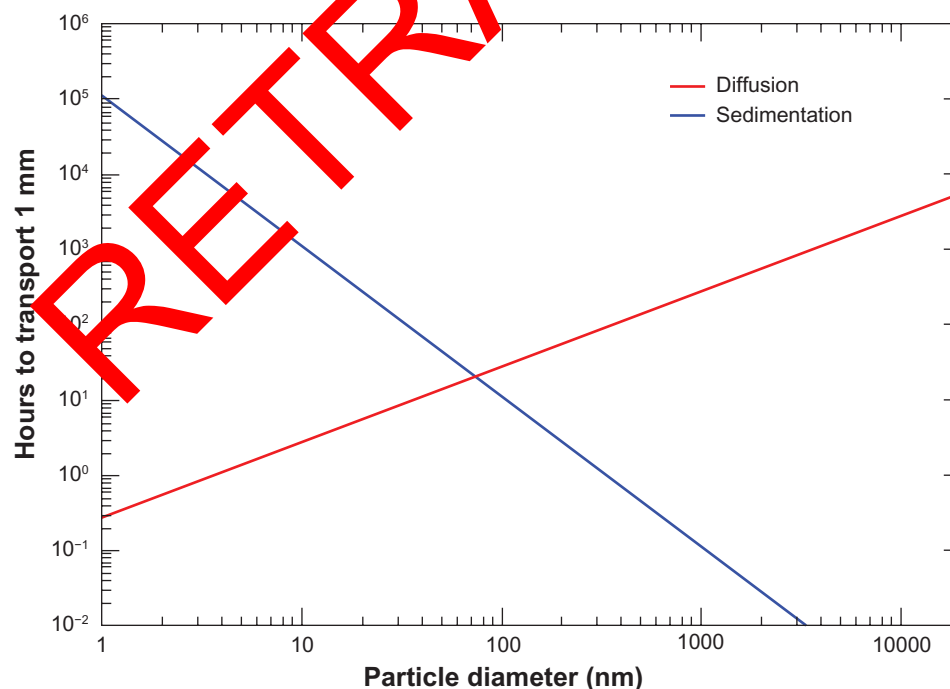


Figure 3 Transport time of magnetite particle to propagate 1 mm in terms of particle diameter.

Notes: Transport is represented for diffusion (red line) and sedimentation (blue line) in an aqueous solution. The 1 mm distance is the mean depth for a culture medium used frequently in in vitro evaluation of intracellular labeling. The intersection point of both types of transport is about 75 nm in diameter for a Fe_3O_4 particle.

is specific in in vitro systems, and when compared with other types of soluble particles, is not simple. Thus, there is a need to develop a more complete understanding of all the processes involved, such as the characteristics of the nanoparticles and how the environment affects their physico-chemical properties. For example, particles of different size and density have different deposition rates. This difference corresponds to a distinct method of transport for adherence to cells in culture.²⁴

Formation of agglomerates

Depending on the random movement of SPIONs in suspension, minor particles with low stability may collapse forming larger agglomerates with a density that is lower than that of their primary constituent particles.^{25,26} Magnetic nanoparticles 1–100 nm in size have a higher tendency to form agglomerates. These agglomerated systems affect the shape, density, and size of the particles, as well as their corresponding diffusion and sedimentation processes.^{24,26} As a result of van der Waals and electrostatic forces, these agglomerates tend to bond to each other.²⁷ The SPION agglomerate is thermal when caused by Brownian movement and kinetic if produced by external forces, such as gravity, an electromagnetic field, or aerodynamic effects. It is important to show how these SPION agglomerates interfere with the cell culture medium. The diameter (d_a) and density (ρ_a) of the agglomerate are obtained according to the number of primary particles per agglomerate formed (NP), the packing factor (PF), the fractal dimension (DF), and the porosity (ϵ_a):²⁸

$$d_a = d_p \left(\frac{NP}{PF} \right)^{1/DF} \quad (4A)$$

$$\rho_a = (1 - \epsilon_a) \rho_p \quad (4B)$$

$$\epsilon_a = \left(\frac{d_a}{d_p} \right)^{DF-3} \quad (4C)$$

The velocity of sedimentation depends on the concentration and mobility of the agglomerates. The mobility is inversely proportional to the diameter. Very small particle agglomerates may lead to larger ones very quickly as the period of time in suspension increases. The sedimentation velocity of the agglomerate is given by the expression:²⁸

$$V_a = \frac{(\rho_a - \rho_f)}{18\mu} g d_p^{3-DF} d_a^{DF-1} \quad (5)$$

where DF is the parameter that depicts how primary SPIONs fill up the volume occupied by the agglomerate. Their fractal nature is determined by the flocculation processes causing formation of the agglomerate. Likewise, the packing factor reflects the absence of a porous space in the agglomerate. The packing factor is determined by the monomers formed and how these are arranged in the agglomerate system. The fractal nature of the agglomerate, represented by the fractal dimension ($1 < DF < 3$), is generally more important in determining the density and porosity than the packing factor ($0 < PF < 1$).²⁸ A fractal dimension value of three symbolizes a perfect sphere, with less or no fractal structure and a null porosity level (ie, no liquid stored).

Agglomerate complexes have a larger mass and volume than individual particles. Also, increased gravity, settling, and thrust forces acting proportionally on their structures. These formations are not solid particles because of the spaces between the packed individual particles and therefore have a smaller density and surface area.²⁸ Deposition of agglomerates are commonly larger when compared with primary minor particles, but can be larger or smaller than one primary particle of a comparable size depending on shape and packing density.²⁹

Computational modeling of deposition process

The particles can be transported into cells by diffusion or sedimentation.^{24,30} Particle deposition involves transport of particles in a liquid suspension medium and is analyzed according to the balance between diffusion and gravitational sedimentation. These processes are related by a one-dimensional convection-diffusion equation (6). The equation is a parabolic-type partial differential equation derived from the mass conservation principle and Fick's laws of diffusion:

$$\frac{\partial C(z,t)}{\partial t} = D \frac{\partial^2 C(z,t)}{\partial z^2} - V \frac{\partial C(z,t)}{\partial z} \quad (6)$$

Where $C(z,t)$, represents the concentration of particles in suspension located at a determined height of the recipient (z) in a time instant (t). The first term of the right side corresponds to normal diffusion, while the second describes gravitational sedimentation (convection), and the term of the left side is the temporal variable. The coefficients D and V (diffusion and settling velocity coefficients) relate to the physical characteristics, nanoparticles, and medium corresponding to the problem. These parameters are determined

by the Stokes Law (2) and the Stokes–Einstein (3) equations, respectively.

Equation (6) brings out a high number of solutions. The convection-diffusion equation reflects the problem if the following initial conditions are assumed:

$$C(z, 0) = C_{init}, \quad (7A)$$

$$D \frac{\partial C(z, t)}{\partial z} \Big|_{z=L} = VC(L, t), \quad (7B)$$

$$C(0, t) = 0. \quad (7C)$$

Equation (7A) represents the initial condition of a uniform concentration, (7B) the condition of the convective type at the bottom of the recipient, and (7C) the contour condition when $z = 0$. Above, C_{init} is the initial concentration for $t = 0$.

Numerical solution of convection-diffusion equation

The finite difference method was adopted for one-dimensional resolution of the partial differential equation (6). This method is extremely suitable for problems that reflect transient system behavior. Initially, the domain and derived discretizations are required, and they appear in the partial differential equation represented as quotients of the differences in the variables for additional conditions and contour (7). Approximation of the derivatives are made by applying the Taylor series of the solution function, $C(z, t)$:

$$C(z_0 \pm \Delta z) = C(z_0) \pm \frac{\Delta z}{1!} \frac{\partial C(z)}{\partial z} \Big|_{z_0} + \frac{(\Delta z)^2}{2!} \frac{\partial^2 C(z)}{\partial z^2} \Big|_{z_0} \pm \frac{(\Delta z)^3}{3!} \frac{\partial^3 C(z)}{\partial z^3} \Big|_{z_0} + \dots \quad (8)$$

From the Taylor series combinations, the expressions for the first and second derivatives are obtained. Considering first-order and second-order approximations, these expressions are given by:

$$\frac{\partial C}{\partial z} \Big|_{i,j} = \frac{C_{i+1}^j - C_{i-1}^j}{2\Delta z} + O(\Delta z)^2, \quad (9A)$$

$$\frac{\partial^2 C}{\partial z^2} \Big|_{i,j} = \frac{C_{i+1}^j - 2C_i^j + C_{i-1}^j}{(\Delta z)^2} + O(\Delta z)^2, \quad (9B)$$

$$\frac{\partial C}{\partial t} \Big|_{i,j+1} = \frac{C_i^{j+1} - C_i^j}{\Delta t} + O(\Delta t). \quad (9C)$$

In the previous mentioned equations, $C_i^j = C(z_0 + i\Delta z, t_0 + j\Delta t)$ is the solution function in a discrete form of the convective-diffusion equation for subindices $i = 0, 1, 2, \dots, N$, and Δz is the size of the step in space, likewise with superindices $j = 0, 1, 2, \dots, M$, that represent the nodal points in time, $0, \Delta t, 2\Delta t, \dots, M\Delta t$. Δt is the temporal size step and $M\Delta t (=T_{tot})$ is exposure time. This computational model was developed based on the implicit method of Crank–Nicolson. This method rests on the approximation averages with central differences in spatial and temporal derivatives. So, the final expression of the convection-diffusion discrete form is:

$$\frac{C_i^{j+1} - C_i^j}{\Delta t} = D \left[\frac{1}{2} \left(\frac{C_{i+1}^{j+1} - 2C_i^{j+1} + C_{i-1}^{j+1}}{\Delta z^2} + \frac{C_{i+1}^j - 2C_i^j + C_{i-1}^j}{\Delta z^2} \right) \right] - V \left[\frac{1}{2} \left(\frac{C_{i+1}^{j+1} - C_{i-1}^{j+1}}{2\Delta z} + \frac{C_{i+1}^j - C_{i-1}^j}{2\Delta z} \right) \right]. \quad (10)$$

Where the first and second terms on the right side represent diffusion and gravitational sedimentation processes (6).

Computer simulation and implementation

The Clark–Nicolson algorithm was applied for discretization of the convection-diffusion expression. This algorithm has a second-order error in spatial and temporal discretizations. The algorithm is implemented in FORTRAN 90 language and solves the convection-diffusion equation in $N + 1$ nodal points, constituting in each time step, Δt , a tridiagonal system of $N + 1$ linear equations with $N + 1$ variables. The tridiagonal system may be solved with interactive methods or algorithm patterns for the resolution of tridiagonal systems.³¹ The convective-diffusion equation was transformed into a dimensionless form using the following dimensionless variables for effective and stable computational software:

$$\bar{z} = \frac{z}{L}, \quad \bar{t} = \frac{tV}{L}, \quad \bar{D} = \frac{D}{VL}, \quad \bar{C}(z, t) = \frac{C(z, t)}{C_{init}} \quad (11)$$

and produces the dimensionless partial differential equation:

$$\frac{\bar{C}_i^{j+1} - \bar{C}_i^j}{\Delta \bar{t}} = \bar{D} \left[\frac{1}{2} \left(\frac{\bar{C}_{i+1}^{j+1} - 2\bar{C}_i^{j+1} + \bar{C}_{i-1}^{j+1}}{\Delta \bar{z}^2} + \frac{\bar{C}_{i+1}^j - 2\bar{C}_i^j + \bar{C}_{i-1}^j}{\Delta \bar{z}^2} \right) \right] - \left[\frac{1}{2} \left(\frac{\bar{C}_{i+1}^{j+1} - \bar{C}_{i-1}^{j+1}}{2\Delta \bar{z}} + \frac{\bar{C}_{i+1}^j - \bar{C}_{i-1}^j}{2\Delta \bar{z}} \right) \right]. \quad (12)$$

In a very similar manner, initial conditions and contour in the dimensionless form:

$$\bar{C}_i^{j=0} = 1, \quad (13A)$$

$$\bar{D} \left(\frac{\bar{C}_{N+1}^j - \bar{C}_{N-1}^j}{2\Delta\bar{z}} \right) = \bar{C}_N^j, \quad (13B)$$

$$\bar{C}_{i=0}^j = 0. \quad (13C)$$

Solving (12) through the computational procedure and applying the initial conditions and contour (13), the normalized concentration of SPION profiles are shown for each height level of the recipient over different intervals of exposure time (Figure 4). The decreasing temporal variation of the SPION concentration is observed as a result of deposition at the bottom of the recipient according to diffusion and gravitational sedimentation. In the simulation, the particle diameter and mean height were 50 nm and 4 mm, respectively. The black

circles indicate the mean concentration related to exposure time, and $h(t)$ depicts the decrease in SPION concentration over the period of time, t , as shown in Figure 2. For the calculations, we used the step sizes in coordinate space $\Delta z = 10^{-3}$, and the time step considered was $\Delta t = 10^{-6}$. Our results and analysis are based on the size of the SPIONs, given that the experimental results reported in the literature indicate that particle size in the nanometer range is the most important factor determining the amount of material entering cells.^{32,33}

Characteristics of SPIONs and culture medium

As already mentioned, specific characteristics of SPIONs and culture medium are as follows: SPIONs have their crystalline phase identified as magnetite (Fe_3O_4) covered with dextran at an iron concentration of 20 $\mu\text{g/mL}$; Dulbecco's Modified Eagle's Medium (DMEM) with low glucose (pH 7.4). DMEM contains amino acids, vitamins, non-organic salts, and other components.

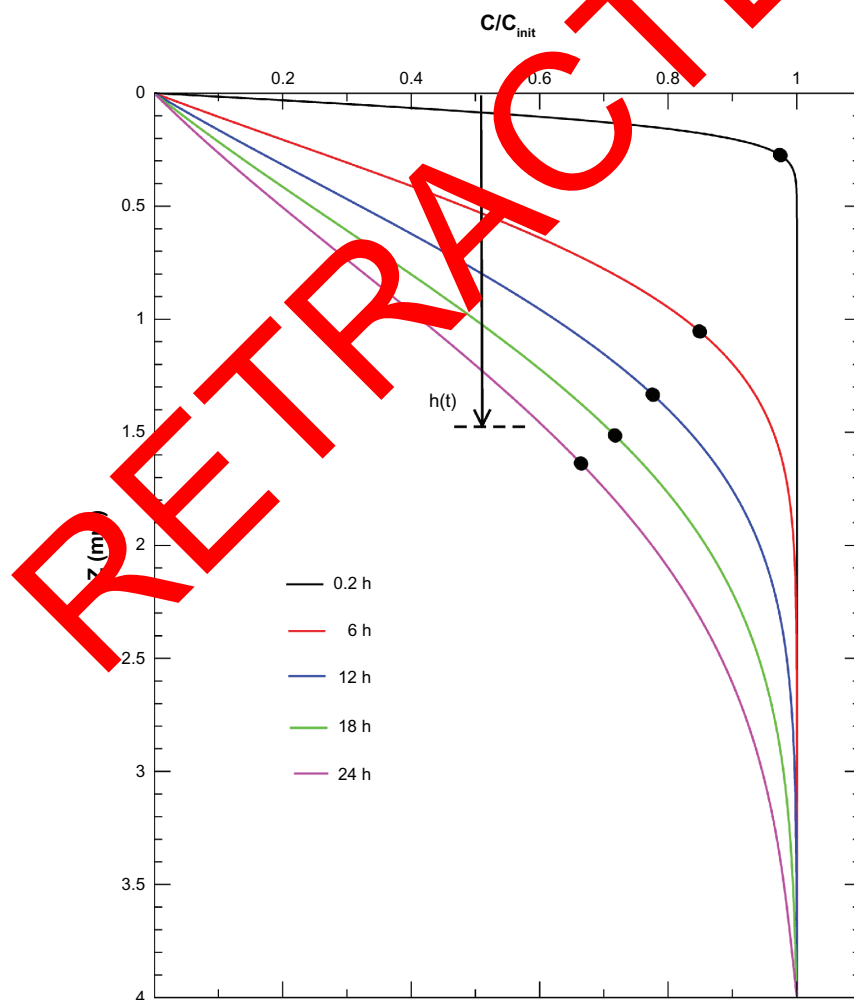


Figure 4 Normalized concentration profiles obtained by the Crank–Nicolson algorithm for resolution of the convection-diffusion equation at different time exposure intervals.

Important parameters of SPIONs and culture medium in this study are: density 5.1 g/cm^3 ; viscosity $8.9 \times 10^{-4} \text{ Pa.s}$; medium density 1.0 g/cm^3 ; media height and temperature 310 K .

Fraction of dose deposited

In order to validate our mathematical simulation method, an experimental imaging study was performed to determine the fraction of nanoparticles deposited. Temporal variation in the concentration of the fraction deposited was determined using SPION phantoms dispersed in the culture medium (Figure 2). Relaxometric measures were used according to the method described by Boutry et al.³⁴

Relaxometric measurements

The images were acquired using a 3.0 Tesla Magnetom Trio (Siemens®, Erlangen, Germany) scanner with a 32-channel coil head in the Department of Magnetic Resonance Imaging at Albert Einstein Hospital. T2-weighted proton slices (each slice of 0.5 mm thickness) were acquired with a multicontrast turbo spin echo. T2-weighted slices were acquired with a repetition time of 1700 ms and an echo time of 101 ms . The matrix size was 256×256 and the field of view was 300 mm . Images were acquired at different periods (1.3 , 5 , 9.7 , and 17.5 hours). All SPION samples were prepared in pairs of 50 nm and 200 nm in diameter, and suspended in DMEM supplemented with 10% fetal bovine serum with an iron concentration of $20 \text{ } \mu\text{g/mL}$. For the control sample, we used a phantom containing DMEM supplemented with 10% fetal bovine serum. The relaxation times (T_2) were measured by images obtained with the sequence of multicontrast turbo spin echo and a phantom height of 4 mm . The relaxation time (T_2) of each sample was calculated by adjusting the decay curve using a monoexponential linear algorithm:

$$\text{signal}_{\text{SE}} = S_0 \exp(-T_2/T_2)$$

Quantification by magnetic resonance imaging

The concentration of SPIONs in solution is correlated with the relaxation rate, R_2 ($1/T_2$) in ms^{-1} , and its relaxivity, r_2 ($\text{ms}^{-1}\text{mL}/\mu\text{g}$). Relaxivity is an intrinsic property of SPIONs which depends on the intensity of the magnetic field. Thus, the iron concentration associated with each relaxation rate, R_2 , measured over determined periods of time ($t_i = t_1, t_2, t_3, \dots, t_n$) can be expressed as:

$$[\text{Fe}]_{i=t_0, t_1, t_2, \dots, t_n} = \frac{(R_2)_{i=t_0, t_1, t_2, \dots, t_n} - (R_2^{\text{CM}})}{r_2}, \quad (14)$$

where r_2 represents the previously determined relaxivity value, $[r_2 = (20.2 \pm 0.4) \times 10^{-4} \text{ ms}^{-1}\mu\text{g}^{-1} \text{ mL}]$, R_2 represents the relaxation rate in suspension, and R_2^{CM} represents the relaxation rate of the culture medium.

The dose fraction deposited at different intervals is determined by:

$$1 - [\text{Fe}]_{t_i} / [\text{Fe}]_{t_0}$$

where $[\text{Fe}]_{t_0}$ is the initial concentration. The iron oxide concentrations were obtained from (14).

Results and discussion

The convection-diffusion equation was resolved based on mathematical modeling of SPION (Fe_3O_4 magnetite) deposition in cell culture medium. The following parameters were used for all calculations: $T = 310 \text{ K}$, $\rho_f = 1.0 \text{ g/cm}^3$, $\rho_p = 5.10 \text{ gr/cm}^3$, and $\mu = 8.9 \times 10^{-4} \text{ Pa.s}$. In addition, specific parameters can be observed for special conditions in the figures presented. Temporal variations in the normalized concentration, $C(z, t)/C_{\text{init}}$, of SPIONs in culture medium were evaluated for different sizes ranging between 5 nm and 500 nm . The agglomerates constituted by different numbers of primary SPIONs ($1-10000$ of Fe_3O_4) were related to exposure time and media height ($1-10 \text{ mm}$) function. The legends show values for specific parameters used in each particular simulation.

The profiles of normalized SPION concentrations are shown in terms of time exposure for defined SPION sizes (Figure 5). The results indicate that the behavior for nanoparticles up to 50 nm in diameter is different from that of particles with larger diameters. A normalized crescent concentration was seen when the size of the nanoparticles was augmented, and an opposite effect was observed for nanoparticles 60 nm or more in diameter (Figure 5A and B). This type of behavior is clearly shown in Figure 3 where a particle with a diameter less than 50 nm took 7 hours to move 1 mm by diffusion and 177 hours by sedimentation, showing the advantage of the diffusion effect for a certain deposition level in this size range. The behavior of SPIONs with a diameter greater than 50 nm may be understood by analyzing the gravitational factor (4) and its influence (3), the latter being favored because of its dependency on d^2 . If we exclude the convective term, the diffusion process is the main mode of transport for SPIONs smaller than 50 nm in diameter.

Calculation of the fraction of the deposited dose $[C_{\text{init}} - C(h(t))/C_{\text{init}}]$ where C_{init} is the initial concentration in

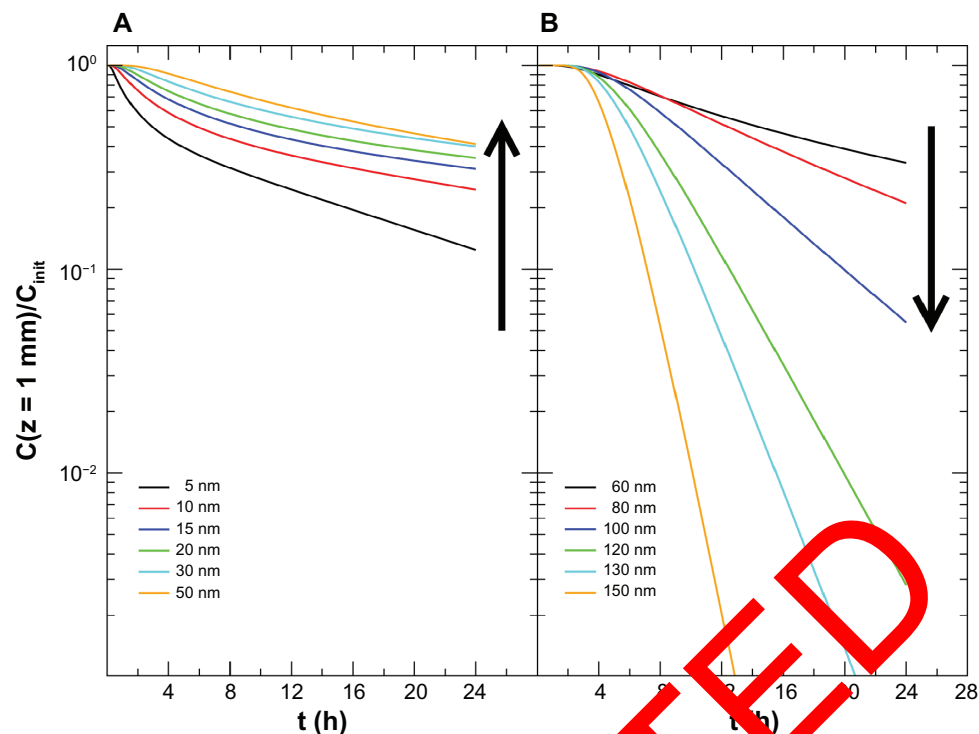


Figure 5 Temporal normalized concentration variability of superparamagnetic iron oxide nanoparticles at $z = 1$ mm during 24 hours of exposure and considering a mean height of 4 mm.

terms of time exposure for SPIONs with a diameter ranging between 5 nm and 500 nm is shown in Figure 6. As in the results observed in Figures 4 and 6 it shows a differentiated behavior pattern for SPIONs with a diameter less than 50 nm. The reason for this is that these nanoparticles are influenced mainly by gravitational sedimentation, while the smallest are controlled by diffusion. Total deposition occurs for larger SPIONs (>150 nm in diameter) by 24 hours.

The contributions of diffusion and sedimentation to the fraction deposited can be seen in Figure 6 by comparing the simulations presented for SPIONs 5–500 nm in diameter (full color lines) with the simulations presented in dashed lines, the latter obtained by considering only the diffusion term in (6). The comparison shows that the diffusion effect dominates completely for smaller SPIONs (25 nm, red line), and competition between these two effects is observed for larger SPIONs (50 nm, green line). For larger particles (eg, 500 nm), represented by the brown line, SPION deposition is dominated by the effect of sedimentation.

We compared our theoretical results with our experimental data, using MRI to determine the fraction of the SPION dose deposited at different exposure times. The experiment was carried out using SPIONs of 50 nm and 200 nm in diameter. Figure 7 shows a comparison of the numerical results for the experimental data, and it can be seen that the

theoretical curve follows the main trend of the experimental data, showing the behavior predicted from the theoretical model.

Significant variation in transport of SPIONs 5–500 nm in diameter according to height was observed. Dose-dependency of the fraction deposited according to mean height (1–10 mm) of the culture medium (distance between surface of culture medium and cells) for different SPION sizes was calculated for a 24-hour time exposure (Figure 8). Our mathematical data explored the predicted tendencies for the deposited dose. A good example is the three-fold increase in deposition occurring with SPIONs 50 nm in diameter when mean height was reduced from 5.1 mm to 1.1 mm. This result could predict greater cell internalization of the NPs, or which could lead to lysis of labeled cells in vitro tests, depending on the concentration of NPs used in cell labeling.

An unexpected consequence of this relationship is the linear increase in the total dose deposited. A linear increase in mean height leads to a larger mean distance moved by the SPIONs until the target cells are reached. The diffusion time for any distance is a quadratic distance function (1). Thus, the volume and fraction of the increase in the dose deposited does not necessarily increase the equivalent target cell dose. All considered, differences using only the mean heights between the studies might lead to misinterpretation of the compara-

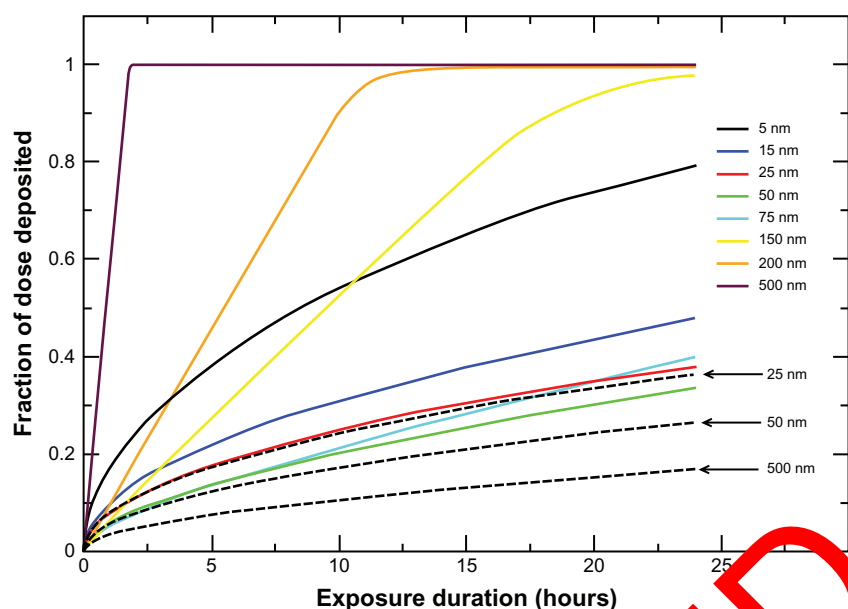


Figure 6 Dose curves of deposited fraction of magnetite nanoparticles (different sizes) in terms of exposure time. **Notes:** All curves were obtained considering a mean height of 4 mm. Dashed lines correspond to equation (6) calculation considering the diffusion factor only.

tive dose-response data. An increase in the volume of the culture medium or dose of nanoparticles administered does not provide equivalent increments in the dose incorporated into the cells.

The fraction of agglomerates of Fe_3O_4 SPIONs ranging between 25 nm and 50 nm in size deposited during a 24-h

exposure period was investigated, and distinct agglomerate systems were formed, with 1–10,000 particles identified for each fraction (Figure 9). For these calculations, we used a packing factor of 0.637 for randomly packed monomers, according to Sterling's work in the absence of experimental value for the packing factor (PF).²⁸ The fractal dimension

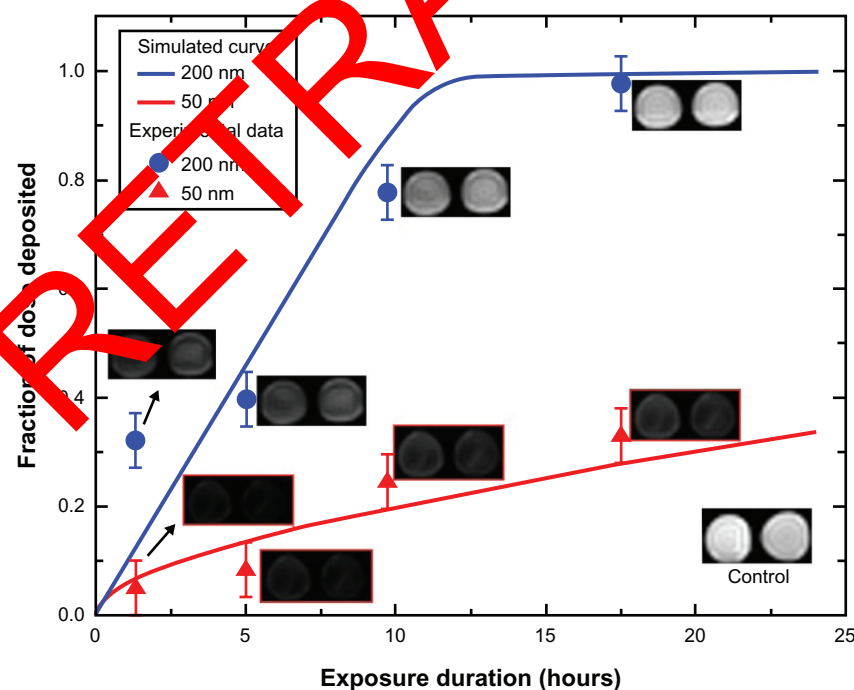


Figure 7 The plotted curves represent the temporal variation in the fraction of dose deposited, with simulated curves for experimental data obtained using magnetic resonance imaging.

Notes: The inset shows images acquired by T2-weighted magnetic resonance imaging of suspensions of superparamagnetic iron oxide nanoparticles 50 nm and 200 nm in diameter in Dulbecco's Modified Eagle's Medium supplemented with 10% fetal bovine serum. The theoretical curves are the same as those shown in Figure 6.

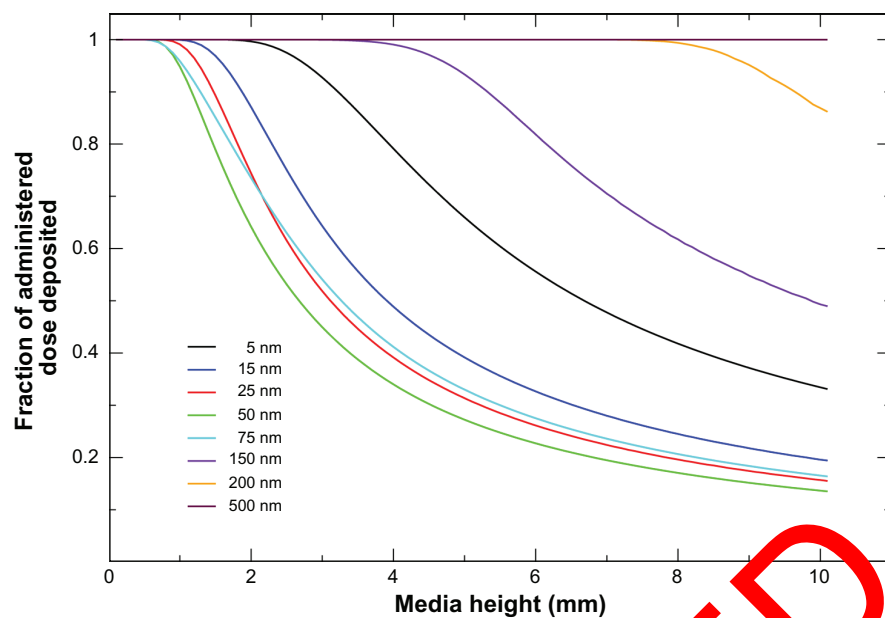


Figure 8 Variability in fraction of the dose deposited on cellular surfaces with a determined: mean of height, suspension volume, and culture medium for superparamagnetic iron oxide nanoparticles of different diameters.

for simulation of SPION agglomerates is still not known. Fractal dimensions of 1 (representing a rod) and 3 (represents a compact sphere) were unlikely, so were not used. The fractal dimensions tested for cerium oxide and silicium dioxide colloids were around 2.^{32,35} Primary nanoparticle agglomerates of smaller diameter show decreased deposition rates, with a less efficient packing factor. Competition between the effect

of diffusion and sedimentation take part in agglomerate suspensions, and a similarly decreased deposition rate with increasing nanoparticle size was observed (Figures 6 and 9). In a complex containing a higher number of agglomerates, the deposition rate shows crescent behavior in terms of nanoparticle size, where an efficient packing level would produce similar behavior for the primary nanoparticles.

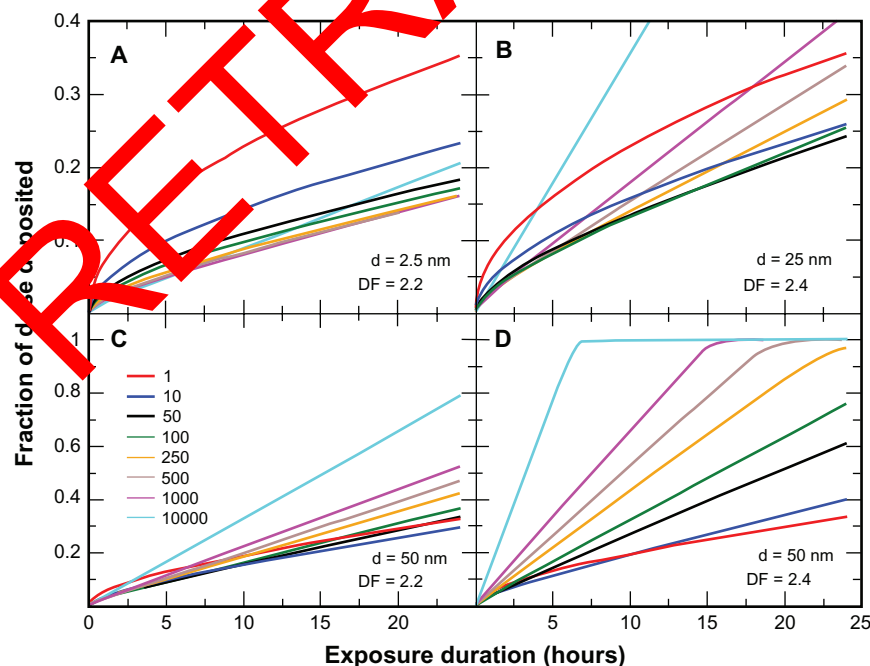


Figure 9 Fraction of dose deposited per agglomerate of primary superparamagnetic iron oxide nanoparticles (Fe_3O_4) during 24 hours of exposure with a mean height of 4 mm. Simulated curves for primary nanoparticles 25 nm in diameter (A and B) and 50 nm (C and D).

Note: Each line represent a different number of nanoparticles per agglomerate (1, 10, 50, 100, 250, 500, 1000, and 10,000), with varying DF values.

In Figure 9, we show the behavior of the deposited dose of agglomerates formed by primary Fe_3O_4 SPIONs with diameters of 25 nm and 50 nm, considering different values for the packing factor, ie, 2.2 and 2.4. In the simulations, the deposition rates decrease with the size of the cluster when the packing factor is less efficient (Figure 9A and C). Increased efficiency of packaging or filling of the cluster increases the sedimentation rate (Figure 9B and C). Competition between diffusion and sedimentation is also present in suspensions with clusters, with the same pattern of decreasing deposition rate with increasing SPION size, as shown in Figure 6 for the primary Fe_3O_4 SPIONs. Figure 9B shows the decrease in deposition rate with increasing numbers of aggregates in an agglomerate containing 50 SPIONs. For agglomerates containing a larger number of aggregates, the deposition rate tends to increase with the size of the nanoparticles. Efficient packing in the agglomerate would result in very similar behavior to that of the primary nanoparticles.

The diffusion coefficient, D , is a physicochemical property of the particle. It is not constant and can vary with changes in concentration, temperature, pressure, solvent properties, and chemical nature of the diffusant. The diffusion coefficient was considered a constant in all simulations, but we also analyzed the effect of the deposition rate using a diffusion coefficient depending on time. We assume that temporal variation of the diffusion coefficient may have

the following characteristic: $D(t) = D_0 f(mt)$, where m is a constant with an inverse dimension to the temporal variable (h^{-1}), $f(mt)$ is a dimensionless expression for the mt variable, and D_0 may be defined as the initial diffusion coefficient. The function $f(mt)$ was chosen in two situations: $f(mt) = 1$ and $m = 0$ or $t = 0$, the first depicting uniform nanoparticle diffusion and the second represents the initial diffusion. The function $f(mt)$ is presumed to be an exponential type: $f(mt) = \exp(mt)$, assuming that $m = 0.05 \text{ h}^{-1}$ considers the crescent and decrescent nature of the function $f(mt)$.

In Figure 10, SPIONs 50 nm in diameter were tested for different diffusion coefficients, with deposited dose fraction curves for distinct exposure times (6, 12, 18, and 24 hours) with $m = 0$ and for a variable diffusion coefficient in terms of crescent and decrescent times ($m = 0.05$), considering an exposure period of 24 hours (solid black line). Particles of greater size did not show a significant temporal diffusion effect because of diminished effect of the diffusion process (Figure 5).

The model shown here makes an important contribution to studies of nanoparticles used in biomedical applications. Our results are limited to systems in which the physical characteristics of the nanoparticles and the medium (density, viscosity, temperature, size, volume, and mean height) are dominant factors in the deposition of nanoparticles suspended in an aqueous medium. More realistic calculations using

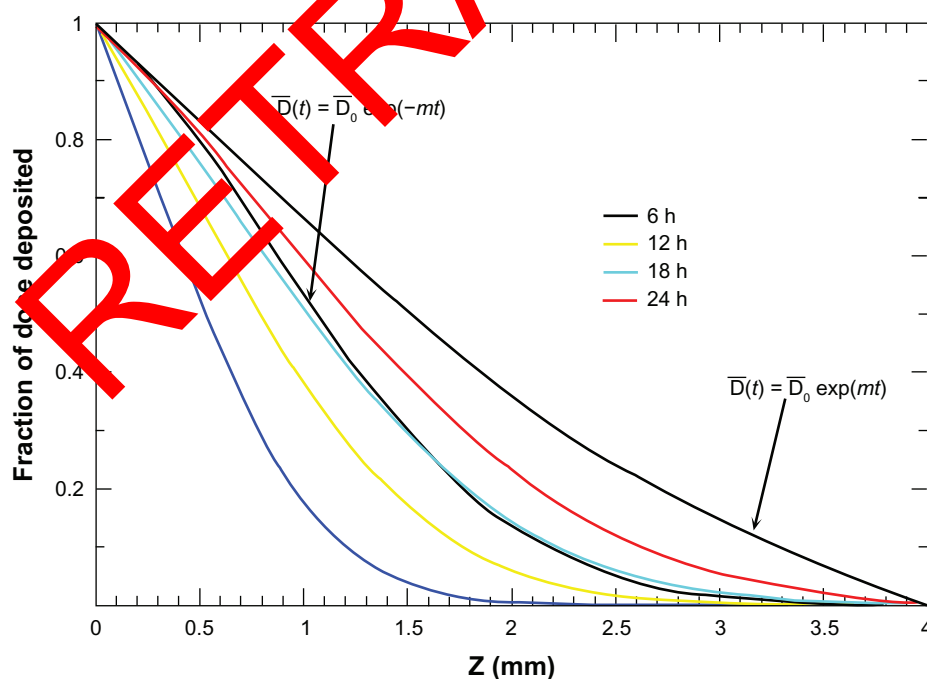


Figure 10 Dose fraction curves for superparamagnetic iron oxide nanoparticles 50 nm in diameter deposited over 6, 12, 18, and 24 hours of exposure.

Notes: The concentration profiles increase within duration of exposure and a null m value (blue, orange, cyan and red lines) was applied. Curves with a dispersion factor in terms of time (full black lines) are shown for crescent (mt) and decrescent ($-mt$) dependencies over time $t(\text{h})$. The value adopted for m was 0.05 h^{-1} .

nanoparticles which are engineered differently have to be made, taking into account the stability of the nanoparticle dispersion and analysis of electrostatic forces, steric, magnetic dipole, ionic strength, van der Waals interactions, and pH of the medium.

Conclusion

In the present work, the convection-diffusion equation was resolved using the finite differences method via the Crank–Nicolson algorithm. Concentration profiles were obtained for SPIONs suspended in a liquid with the characteristics of a culture medium. This system involves in vitro sedimentation, which is widely used for cell internalization and toxicity studies. Calculations for different SPION sizes and mean heights in culture medium are simulated. Based on this experiment, using data acquired by MRI, we have confirmed the acuity of the mathematical modeling approach to determine the behavior of SPIONs suspended in DMEM.

The concentration profiles obtained show crescent-type behavior in terms of SPION size (up to 50 nm in diameter) whereby the diffusion effect prevents the opposite behavior by larger particles with a larger sedimentation effect. The effect of sedimentation is also found in the fraction of deposited dose. Complete SPION deposition occurred for nanoparticles larger than 150 nm within a 24-hour time period. Agglomerated simulations were achieved and the deposition rate decreased because of an agglomerate size with less efficient packing factor. Competition between diffusion and sedimentation effects was also observed in suspensions containing agglomerates. An efficient agglomerate packing level produces behavior similar to that of primary nanoparticles.

Our analyses show significant variations in the deposited dose in accordance with the diffusion coefficients which are dependent on time. It was seen that increasing temporal dependence causes faster deposition through the medium. Variation in temporal diffusion causes considerable variation in the deposited dose, i.e., 22% for crescent diffusion and 13% for decrescent diffusion, indicating small alterations in the diffusion coefficient.

The present results are very important for the planning of nanomaterial absorption, providing information for efficient intracellular labeling and controlling toxicity. This model enables determination of the in vitro transport characteristics of specific SPIONs which would be relevant to other models using cellular components and particle absorption processes.

The results presented here are of great importance in planning nanomaterial absorption, providing information on

efficient intracellular labeling and toxicity related to uptake of magnetic nanoparticles by cells. This model provides an adequate approximation of the expected cell dose as a function of nanoparticle size. The model also allows identification of particle transport patterns to determine whether transport processes are an important factor in the study of in vitro techniques. As shown in our results, in some cases, there is improved diagnostic accuracy for particles with specific and related models that describe cellular processes affecting particle absorption. Our results should guide and/or help interpret future studies of in vitro toxicity and intracellular labeling. The present modeling application may be extended to engineered nanoparticles considering variations in viscosity, chemical surface structure, and ionic and surface charge interactions in the fields of health care and environmental safety.^{36,37}

Acknowledgments

This work was supported by Albert Einstein Israeli Institute of Teaching and Research (IIEPAE). The financial support from the Brazilian agencies: Coordination of Improvement of Higher Education Personnel (CAPES), National Counsel of Technological and Scientific Development (CNPq), Financier of Studies and Projects (FINEP), and São Paulo Research Foundation (FAPESP).

Disclosure

The authors report no conflicts of interest in this work.

References

1. Sousa MH, Rubim JC, Sobrinho PG, Tourinho FA. Biocompatible magnetic fluid precursors based on aspartic and glutamic acid modified maghemite nanostructures. *J Magn Magn Mater*. 2001;225:67–72.
2. Tartaj P, Morales MP, Veintemillas-Verdaguer S, Gonz  les-Carre  o T, Serna CJ. The preparation of magnetic nanoparticles for applications in biomedicine. *J Phys D Appl Phys*. 2003;36:R182–R197.
3. Gupta AK, Wells S. Surface-modified superparamagnetic nanoparticles for drug delivery: preparation, characterization, and cytotoxicity studies. *IEEE Trans Nanobioscience*. 2004;3:66–73.
4. Kopelman R, Koo Y-EL, Philbert M, et al. Multifunctional nanoparticle platforms for in vivo MRI enhancement and photodynamic therapy of a rat brain cancer. *J Magn Magn Mater*. 2005;293:404–410.
5. Bonnemain B. Superparamagnetic agents in magnetic resonance imaging: physicochemical characteristics and clinical applications. *J Drug Target*. 1998;6:167–174.
6. Kircher MF, Allport JR, Graves EE, et al. In vivo high resolution three-dimensional imaging of antigen-specific cytotoxic T-lymphocyte trafficking to tumors. *Cancer Res*. 2003;63:6838–6846.
7. Wu EX, Tang HY, Wong KK, Wang J. Mapping cyclic change of regional myocardial blood volume using steady-state susceptibility effect of iron oxide nanoparticles. *J Magn Reson Imaging*. 2004;19: 50–58.
8. Bachmann R, Conrad R, Kreft B, et al. Evaluation of a new ultrasmall superparamagnetic iron oxide contrast agent Clariscan[ ], (NC100150) for MRI of renal perfusion: experimental study in an animal model. *J Magn Reson Imaging*. 2002;16:190–195.

9. Alger JR, Harreld JH, Chen S, Mintonovitch J, Lu DSK. Time-to-echo optimization for spin echo magnetic resonance imaging of liver metastasis using superparamagnetic iron oxide particles. *J Magn Reson Imaging*. 2001;14:586–594.
10. Wilhelm C, Gazeau F, Roger J, Pons JN, Bacri J-C. Interaction of anionic superparamagnetic nanoparticles with cells: kinetic analyses of membrane adsorption and subsequent internalization. *Langmuir*. 2002;18:8148–8155.
11. Portet D, Denizot B, Rump E, Lejeune J, Jallet P. Nonpolymeric coatings of iron oxide colloids for biological use as magnetic resonance imaging contrast agents. *J Colloid Interface Sci*. 2001;238:37–42.
12. Jordan A, Scholz R, Maier-Hauff K, et al. Presentation of a new magnetic field therapy system for the treatment of human solid tumors with magnetic fluid hyperthermia. *J Magn Magn Mater*. 2001;225:118–126.
13. Ito A, Kuga Y, Honda H, et al. Magnetite nanoparticle-loaded anti-HER2 immunoliposomes for combination of antibody therapy with hyperthermia. *Cancer Lett*. 2004;212:167–175.
14. Kong G, Braun RD, Dewhirst MW. Hyperthermia enables tumor-specific nanoparticle delivery: effect of particle size. *Cancer Res*. 2000;60:4440–4445.
15. Ito A, Shinkai M, Honda H, Kobayashi T. Medical application of functionalized magnetic nanoparticles. *J Biosci Bioeng*. 2005;100:1–11.
16. Conner SD, Schmid SL. Regulated portals of entry into the cell. *Nature*. 2003;422:37–44.
17. Nel A, Xia T, Mädler L, Li N. Toxic potential of materials at the nanolevel. *Science*. 2006;311:622–627.
18. Oberdorster G, Oberdorster E, Oberdorster J. An emerging discipline evolving from studies of ultrafine particles. *Environ Health Perspect*. 2005;113:823–839.
19. Morrison ID, Ross S. *Colloidal Dispersions: Suspensions, Emulsions, and Foams*. New York, NY: Wiley-Interscience; 2002.
20. Teeguarden JG, Hinderliter PM, Orr G, Thrall BD, Pounds JG. Particokinetics in vitro: dosimetry considerations for in vitro nanoparticle toxicity assessments. *Toxicol Sci*. 2007;95:300–312.
21. Zhang S, Li J, Lykotrafitis G, Bao G, Suresh S. Size-dependent endocytosis of nanoparticles. *Adv Mat*. 2008;20:1–6.
22. Conner SD, Schmid SL. Regulated portals of entry into the cell. *Nature*. 2003;422:37–44.
23. Decuzzi P, Ferrari M. The receptor-mediated endocytosis of nonspherical particles. *Biophys J*. 2008;94:3770–3797.
24. Cho EC, Zhang Q, Xia Y. The effect of sedimentation and diffusion on cellular uptake of gold nanoparticles. *Nat Nanotechnol*. 2011;6:385–391.
25. Sayes CM, Reed KR, Warheit DB. Assessing toxicity of fine and nanoparticles: comparing in vitro measurements to in vivo pulmonary toxicity profiles. *Toxicol Sci*. 2007;97:163–180.
26. Kato H, Suzuki M, Fujita K, et al. Reliable size determination of nanoparticles using dynamic light scattering method for in vitro toxicology assessment. *Toxicol In Vitro*. 2009;23:927–934.
27. Frienlander SK, Pui D. NSF workshop report on emerging issues. In: *Nanoparticle Aerosol Science And Technology*. Los Angeles, CA: University of California; 2003.
28. Sterling MC, Bonner JS, Ernest AN, Page CA, Autenrieth RL. Application of fractal flocculation and vertical transport model to aquatic sol-sediment systems. *Water Res*. 2005;39:1818–1830.
29. Johnson CP, Li X, Logan BE. Settling velocities of fractal aggregates. *Environ Sci Technol*. 1996;30:1911–1918.
30. Gregory J. *Particles in Water: Properties and Processes*. London, UK: Taylor and Francis; 2006.
31. Press WH, Teukolsky SA, Vetterling WT, Flannery BP. *Numerical Recipes in Fortran, The Art of Scientific Computing – Second Edition*. Cambridge University Press, New York, 1992;1:42.
32. Limbach LK, Li Y, Gray RN, et al. Oxide nanoparticle uptake in human lung fibroblasts: effects of particle size, agglomeration, and diffusion at low concentrations. *Environ Sci Technol*. 2005;39:9370–9376.
33. Sun W, Fang N, Treanor LB, Tsunoda M, Lin VS, Yeung ES. Endocytosis of a single mesoporous silica nanoparticle into a human lung cancer cell observed by differential phase contrast microscopy. *Anal Bioanal Chem*. 2008;361:2119–2125.
34. Pothier S, Forgey B, Burtea C, et al. How to quantify iron in an aqueous or biological matrix: a technical note. *Contrast Media Mol Imaging*. 2009;4:299–304.
35. Bergna HE, Roberts WO, editors. *Colloidal Silica: Fundamentals and Applications*. Boca Raton, FL: CRC Press, Taylor and Francis Group; 2006.
36. Smoluchowski MV. Theoretische Bemerkungen über die Viskosität der Kolloide (Theoretical remarks on the viscosity of the colloids). *Colloid and Polym Sci*. 1916;18(5):190–195.
37. Heine DR, Petersen MK, and Grest GS. Effect of particle shape and charge on bulk rheology of nanoparticle suspensions. *J Chem Phys*. 2010;132(18):184509.

International Journal of Nanomedicine

Publish your work in this journal

The International Journal of Nanomedicine is an international, peer-reviewed journal focusing on the application of nanotechnology in diagnostics, therapeutics, and drug delivery systems throughout the biomedical field. This journal is indexed on PubMed Central, MedLine, CAS, SciSearch®, Current Contents®/Clinical Medicine,

Submit your manuscript here: <http://www.dovepress.com/international-journal-of-nanomedicine-journal>

Dovepress

Journal Citation Reports/Science Edition, EMBase, Scopus and the Elsevier Bibliographic databases. The manuscript management system is completely online and includes a very quick and fair peer-review system, which is all easy to use. Visit <http://www.dovepress.com/testimonials.php> to read real quotes from published authors.